

Working fluids for low-temperature organic Rankine cycles

Bahaa Saleh¹, Gerald Koglbauer, Martin Wendland, Johann Fischer*

Institut für Verfahrens- und Energietechnik, Universität für Bodenkultur, Muthgasse 107, A-1190 Wien, Austria

Received 19 October 2005

Abstract

A thermodynamic screening of 31 pure component working fluids for organic Rankine cycles (ORC) is given using BACKONE equation of state. The fluids are alkanes, fluorinated alkanes, ethers and fluorinated ethers. The ORC cycles operate between 100 and 30 °C typical for geothermal power plants at pressures mostly limited to 20 bar, but in some cases supercritical pressures are also considered. Thermal efficiencies η_{th} are presented for cycles of different types. In case of subcritical pressure processes one has to distinguish (1) whether the shape of the saturated vapour line in the T,s -diagram is bell-shaped or overhanging, and (2) whether the vapour entering the turbine is saturated or superheated. Moreover, in case that the vapour leaving the turbine is superheated, an internal heat exchanger (IHE) may be used. The highest η_{th} -values are obtained for the high boiling substances with overhanging saturated vapour line in subcritical processes with an IHE, e.g., for *n*-butane $\eta_{th} = 0.130$. On the other hand, a pinch analysis for the heat transfer from the heat carrier with maximum temperature of 120 °C to the working fluid shows that the largest amount of heat can be transferred to a supercritical fluid and the least to a high-boiling subcritical fluid.

© 2006 Elsevier Ltd. All rights reserved.

Keywords: Organic Rankine cycle; Working fluids; Low temperature heat; Geothermal power plant

1. Introduction

Presently, there is much effort in using renewable energies like solar energy, wind energy, biomass and geothermal heat as well as in using waste heat for the production of electricity. The organic Rankine cycle (ORC) is a promising process for conversion of low and medium temperature heat to electricity. The ORC process works like a Clausius–Rankine steam power plant but uses an organic working fluid instead of water. A certain challenge is the choice of the organic working fluid and of the particular design of the cycle. The process should have a high thermal efficiency η_{th} and allow a high utilization of the available heat source. Moreover, the working fluid should fulfil safety criteria, it should be environmentally friendly, and allow low cost for the power plant. An

important aspect for the choice of the working fluid is the temperature of the available heat source, which can range from low temperatures of about 100 °C to medium temperatures of about 350 °C. A question, which also has to be considered in discussing ORC-processes, is whether an organic substance is really better than water as working fluid for a given task. This question arises, in particular, for medium temperature heat sources. For low temperature heat sources the advantage of organic fluids is obvious because of the volume ratio of the working fluid at the turbine outlet and inlet. This can be smaller by an order of magnitude for organic fluids than for water and hence allows the use of simpler and cheaper turbines [1].

Here, we concentrate on the production of electricity from low temperature heat sources as, e.g., geothermal heat with a temperature of about 100 °C or somewhat higher. We want to emphasize that geothermal power plants already exist. Examples are the plants in Altheim, Austria, with a power production of 1 MW_{el} [2,3] and in Neustadt-Glewe, Germany, with a power production of 0.2 MW_{el} [4] both of which used initially *n*-perfluoropentane as working fluid [3,4]. This substance, however, bears

*Corresponding author. Tel.: +43 1 3709726 201;
fax: +43 1 3709726 210.

E-mail address: johann.fischer@boku.ac.at (J. Fischer).

¹Present address: Mechanical Engineering Department, Faculty of Engineering, Assiut University, Assiut, Egypt.

several problems. It is environmentally not very friendly because of a very high global warming potential and a high atmospheric lifetime [5]. Moreover, as will be shown here, it has a relatively low thermal efficiency in a simple cycle without internal heat exchanger and the degree of utilization of the available heat source is limited by a high pinch point temperature. Hence, the question arises, whether other working fluids with more favourable properties can be found. The screening of 31 potential pure component working fluids and of different cycles is the content of this paper.

The paper is organized as follows. In Section 2 different types of ORC-processes are discussed which match different thermodynamic properties of the working fluids. In order to calculate the thermodynamic properties and in particular the thermal efficiency, a fundamental equation of state is required. Here BACKONE equation of state is used [6–14]. This equation is shortly reviewed in Section 3 and parameters are given there for 31 pure component working fluids. In Section 4 the thermal efficiencies and other thermodynamic properties of these working fluids in ORC-processes are presented. The fluids operate between 100 and 30 °C typical for geothermal power plants. We consider 67 processes with pressures up to 20 bar and 10 processes with supercritical pressures. In Section 5 we consider the heat transfer from the heat carrier fluid to the working fluid by a pinch analysis for four representative cycles assuming a maximum temperature of the heat carrier of 120 °C. Finally, additional aspects will be discussed and some conclusions are drawn.

2. Different types of ORC cycles

The Clausius–Rankine cycle is known from the standard textbooks of thermodynamics as e.g. [1]. It shall, however, be reviewed here for a clear definition of the different types of ORC cycles to be considered in this paper. An important feature for the classification of ORC cycles is the shape of the saturated vapour line in the temperature versus entropy T,s -diagram. The saturated vapour line may either lead to a bell-shaped coexistence curve like in Figs. 1 or 2 or it may be overhanging like in Fig. 3. Correspondingly we use the notations “b-” for fluids with bell-shaped and “o-” for fluids with overhanging saturation line. An additional aspect for the classification of the ORC cycles is the pressure at which the working fluid takes up heat from the carrier fluid of the heat source. For subcritical pressures (Figs. 1–3) the fluid undergoes a liquid–vapour phase transition process during heating, whilst for super critical pressures (Fig. 4) such a phase transition does not occur. Now, several types of ORC processes can be defined.

b1 cycle: Let us first consider one type of ORC process for the case of a b-fluid which is schematically represented in the T,s -diagram in Fig. 1. The working fluid leaves the condenser as saturated liquid with temperature T_1 and condenser pressure p_{min} (state point 1). Then it is

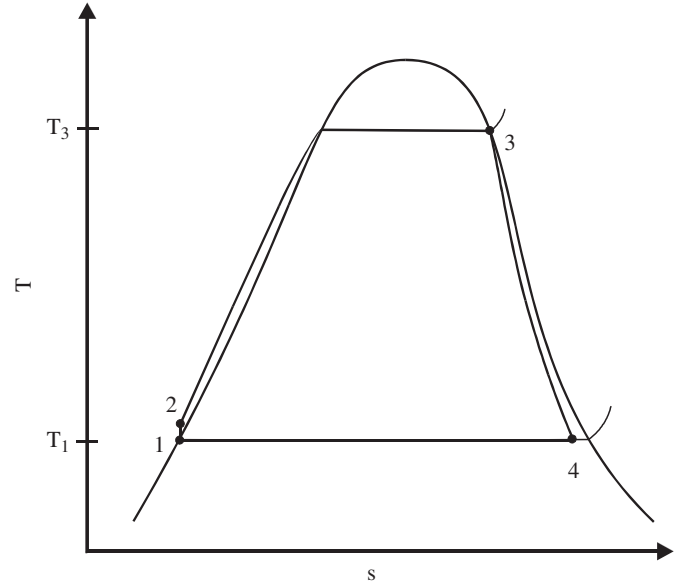


Fig. 1. ORC cycle b1 in the T,s -diagram for a fluid with bell-shaped coexistence curve and saturated vapour at the turbine inlet.

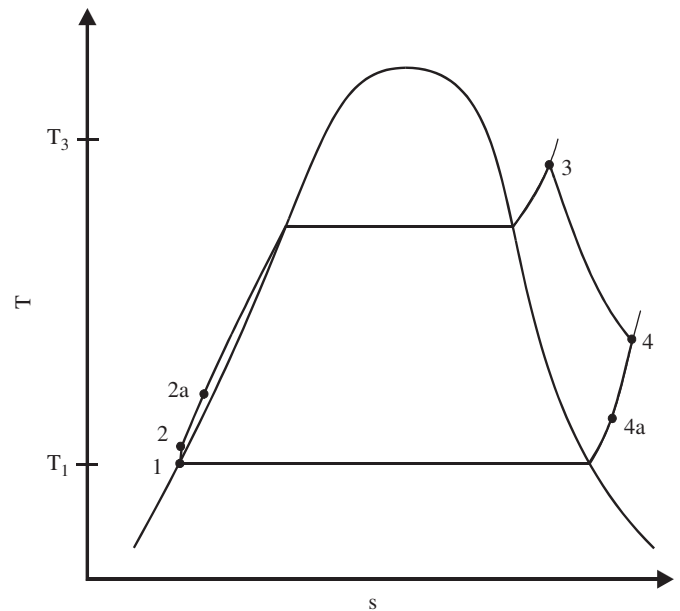


Fig. 2. ORC cycle b3 in the T,s -diagram for a fluid with bell-shaped coexistence curve and superheated vapour at the turbine inlet.

compressed in the feed pump to the subcritical evaporator pressure p_{max} (state point 2) with an isentropic pump efficiency η_{sp} . Then, the fluid is heated in the evaporator at constant pressure till it becomes saturated vapour (state point 3). Thus it enters the turbine and is expanded to the condenser pressure p_{min} arriving at the end of the expansion at state point 4, which lies in the two-phase region. During the expansion the fluid delivers work with an isentropic turbine efficiency η_{sT} . Finally, the fluid passes through the condenser where heat is removed at constant pressure till it becomes a saturated liquid (state point 1).

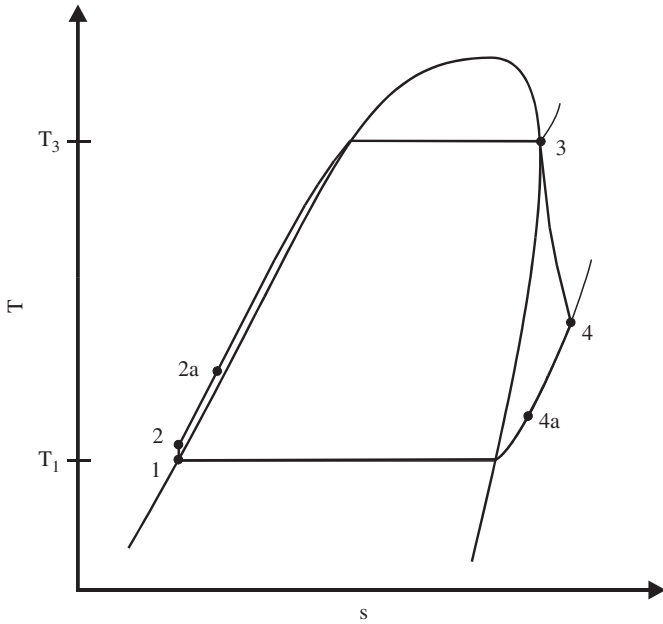


Fig. 3. ORC cycle o2 in the T,s -diagram for a fluid with overhanging coexistence curve and saturated vapour at the turbine inlet.

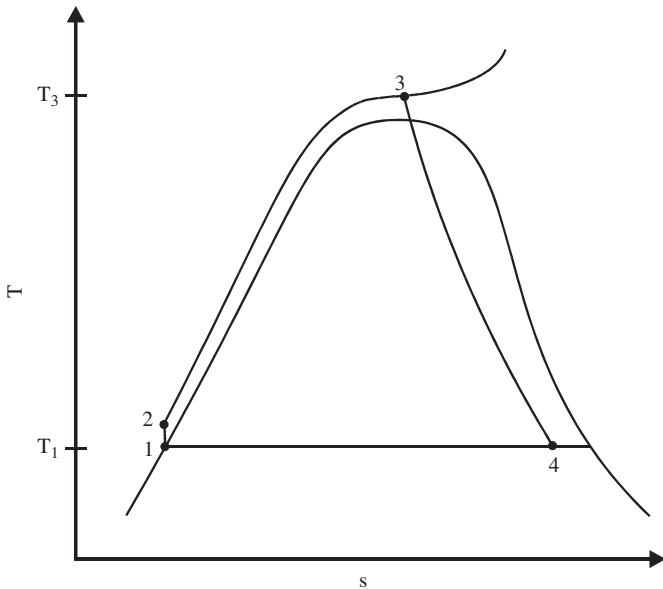


Fig. 4. ORC cycle s1 in the T,s -diagram for supercritical pressure cycle.

b2 cycle: This b-fluid cycle is similar to the b1 cycle with the only difference that the state point 4 after the expansion in the turbine lies in the superheated vapour region.

b3 cycle: Let us consider now an other type of ORC process for the case of a b-fluid which is schematically represented in the T,s -diagram in Fig. 2. The state points 1 and 2 correspond to cycles b1 and b2. Starting from state point 2, the fluid is heated in the evaporator at constant subcritical pressure till it becomes saturated vapour and thereafter it is superheated (state point 3). Then it is expanded with an isentropic turbine efficiency η_{sT} to state point 4, which is in the superheated vapour region as in cycle b2.

o2 cycle: Let us now consider the ORC process for the case of an o-fluid which is schematically represented in the T,s -diagram in Fig. 3. The process steps are the same as in the b2 cycle. Point 3 lies on the saturated vapour line and because this is overhanging point 4 can only be located on the condenser pressure isobar p_{min} in the superheated vapour region.

o3 cycle: The process steps in this o-fluid cycle are the same as in the b3 cycle. Points 3 and 4 are in the superheated vapour region.

s1 cycle: Presently, there are suggestions to pressurize the working fluid to a supercritical pressure p_{max} . Such a cycle is schematically represented in the T,s -diagram in Fig. 4. This process is different from those described above because in heating up the fluid on the supercritical isobar from points 2 to 3 no phase transition takes place and a supercritical compressed fluid enters the turbine. These supercritical cycles can be performed with b- and o-fluids. If the end point of the expansion in the turbine, point 4, is located in the two-phase region we call this an s1 cycle.

s2 cycle: The process steps in this cycle are the same as in the s1 cycle with the only difference that point 4 lies in the superheated vapour region.

In all these cycles the heat q_{23} is added to the working fluid during the process (2–3) and the heat q_{41} is removed from it during the process (4–1). The work w_{34} is taken from the turbine during process (3–4) and a small amount of work w_{12} is required to pump the liquid during the process (1–2). Then the thermal efficiency of the cycle is given as

$$\eta_{th} = - (w_{34} + w_{12}) / q_{23} = - [(h_4 - h_3) + (h_2 - h_1)] / (h_3 - h_2), \quad (1)$$

where $h_1, h_2, h_3,$ and h_4 are the specific enthalpies in the respective state points in Figs. 1–4.

We note, that in the cycles b2, b3 (Fig. 2), o2 (Fig. 3) and s2 the temperature T_4 is higher than the temperature T_1 . In case that T_4 is remarkably higher than T_1 it may be rewarding [15] to implement an internal heat exchanger (IHE) into the cycle as shown in Fig. 5. This heat exchange is also represented in Figs. 2 and 3 by the additional state points 4a and 2a. The vapour cools down in the heat exchanger in the process (4–4a) by transferring the heat q_{44a} without loss to the compressed liquid which is heated up in the process (2–2a) by $q_{22a} = -q_{44a}$. In this case, the thermal efficiency of the cycle is given as

$$\eta_{th} = - (w_{34} + w_{12}) / q_{2a3} = - [(h_4 - h_3) + (h_2 - h_1)] / (h_3 - h_{2a}), \quad (2)$$

where $h_1, h_2, h_{2a}, h_3,$ and h_4 are the specific enthalpies in the respective state points in Figs. 2 and 3.

In order to understand the advantage of the internal heat transfer, two complementary considerations can be made. First, this internally transferred heat does not need to be supplied from outside and hence obviously increases the thermal efficiency. Second, both types of cycles work

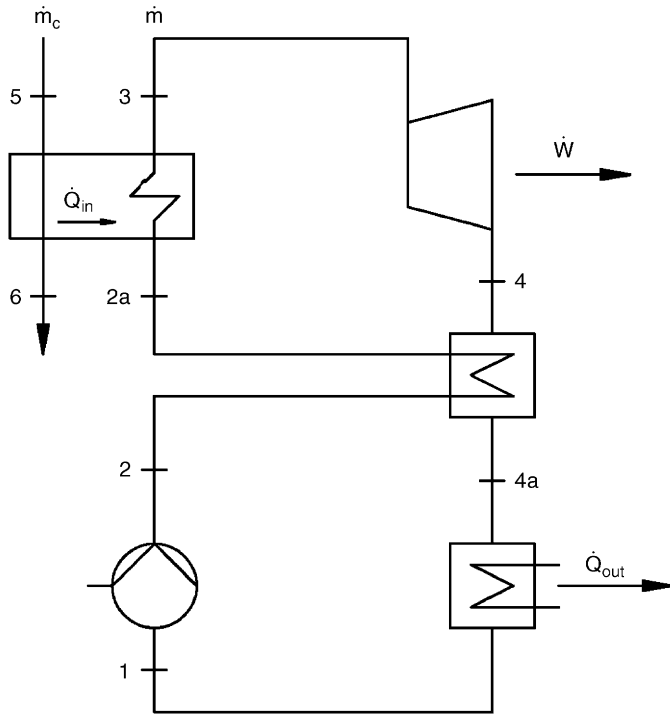


Fig. 5. ORC plant with internal and external heat exchanger.

between the same minimum temperature T_1 and the same maximum temperature T_3 . There are, however, differences in the average temperature at which heat is supplied to the system and in the average temperature at which heat is transferred to the environment. In case with IHE the average temperature of heat transfer to the cycle (from T_{2a} to T_3) is higher than without IHE (from T_2 to T_3) while the average temperature of heat transfer to the environment (from T_{4a} to T_1) is lower than in case without IHE (from T_4 to T_1). Both these differences result according to Carnot in a higher thermal efficiency η_{th} .

An item still to be considered is the supply of the heat flux \dot{Q}_{in} to the working fluid in the evaporator. In general, this heat is supplied from an external heat carrier fluid and the evaporator is the cold side of an external heat exchanger (EHE) as shown in Fig. 5. The ultimate aim in the design of a power plant, however, is not the highest thermal efficiency of the ORC process but rather a maximum power output from a given heat source. This includes consideration of the EHE by a pinch analysis, which has to be based on a $T, \Delta \dot{H}$ -diagram of the working fluid in the evaporator for the different types of ORC cycles.

3. The BACKONE equation of state

In order to evaluate the thermal efficiency η_{th} of a cycle and the $T, \Delta \dot{H}$ -diagram for some working fluid, its thermodynamic properties must be known and described

accurately by a fundamental equation of state (EOS). In this section we will shortly present and discuss the BACKONE equation and give the parameters for 31 pure components to be considered as working fluids for ORC processes.

Most EOS which have a sufficient accuracy as, e.g., those included in REFPROP [16] use a large number of substance specific parameters which need to be fitted to an extensive set of precise experimental data. On the other hand, simple general EOS like cubic EOS have only few parameters and need only a small data base but they do not have sufficient accuracy.

An alternative is the BACKONE equation [6–14]. Strictly speaking, BACKONE is a family of physically based EOS [6], which is able to describe thermodynamic properties of nonpolar, dipolar and quadrupolar fluids with good to excellent accuracy. In BACKONE the Helmholtz energy is written as a sum of contributions from characteristic intermolecular interactions [6]. For nonpolar fluids the Helmholtz energy is given as $F = F_H + F_A$, where F_H is the hard-body contribution, and F_A the attractive dispersion energy contribution. For dipolar fluids the Helmholtz energy is given by $F = F_H + F_A + F_D$, where F_D is the dipolar contribution. For quadrupolar fluids the Helmholtz energy is given by $F = F_H + F_A + F_Q$, where F_Q is the quadrupolar contribution. For many fluids, both the dipolar and quadrupolar contributions have to be considered and hence the Helmholtz energy is written as $F = F_H + F_A + F_D + F_Q$ [8]. The hard body contribution F_H is based on a hard convex body equation which is rewritten as a function of a reduced temperature T/T_0 , a reduced density ρ/ρ_0 , and an anisotropy parameter α which is related to the molecular elongation L . Thus, F_H is a function of temperature T , density ρ , and three substance-specific parameters T_0 , ρ_0 , and α . The attractive contribution F_A is also written as a function of the T , ρ and the same three parameters. The functional form of F_A was found by a simultaneous fit to the experimental data of methane, oxygen and ethane. The quadrupolar and dipolar contributions were both constructed on the basis of extensive molecular simulations. It was assumed that F_D and F_Q depend on T/T_0 , ρ/ρ_0 , and a reduced squared dipole moment μ^{*2} or quadrupole moment Q^{*2} .

Thus, BACKONE requires three to five substance-specific parameters. Because the equation is physically based, only a few experimental saturated liquid density and vapour pressure data are required for determining these substance specific parameters. Moreover, it should be noted that mixing rules for the BACKONE equation are also available [7].

For the calculation of caloric properties as the enthalpy or the entropy, the residual contributions of BACKONE have to be supplemented by ideal gas heat capacities. For most of the working fluids studied here, the ideal gas heat capacities were taken from literature. Otherwise, the Joback method [17] was used to calculate the ideal gas contribution. The Joback method was tested by making comparisons with literature data for many substances.

The deviations of the isobaric ideal gas heat capacities calculated by Joback from literature data are within $\pm 3\%$ for all tested substances.

BACKONE has already been applied to a number of pure natural and HFC refrigerants [6,8–14], which can be used also as working fluids for ORC processes. For natural refrigerants as carbon dioxide, normal, branched or cyclic alkanes and alkenes, one gets the best agreement with experimental data like vapour pressures, saturated liquid densities, saturated vapour densities, pvT-data and caloric data by describing them as quadrupolar fluids [6,8–14]. For HFCs, best agreement is usually obtained with both a dipole and a quadrupole moment [8–10,12].

A further important point is the accuracy of the enthalpies and entropies calculated from BACKONE. Calero et al. [8] showed for R123, R125, R143a, and R152a that BACKONE results for enthalpy and entropy agree with reference EOS within 1.5%. Moreover, for these refrigeration cycles also coefficients of performance (COP) and volumetric refrigeration capacities (VRC) have been checked for pure and mixed natural refrigerants [11] as well as for pure HFC refrigerants [8,12]. For pure fluids, the results of COP and VRC obtained from BACKONE and

from reference EOS compare very well and the deviations are for most pure substances within 1% or very often even much smaller. For mixtures, where no reference EOS are established, the deviations of COP and VRC results from BACKONE and other equations are little higher but still good and within 0.6–2.1%.

In this paper, we consider 31 substances as working fluids for ORC processes for which the BACKONE parameters, their sources and the sources of the ideal gas heat capacities c_p^0 are listed in Table 1. The ordering in this table mainly follows the ASHRAE nomenclature. The BACKONE parameters have been determined elsewhere [8–14] by fitting to vapour pressures and saturated liquid densities. The c_p^0 values were taken for 28 substances from the literature. For the 3 substances R245fa, RE245mc, and RE347mcc they were calculated with the Joback method [17].

The critical temperatures of the substances are given in Table 2 and 3 and range from 44.25 °C for R41 to 234.67 °C for *n*-hexane. This range was determined by the wish to find working fluids for geothermal heat power plants and the assumption that the maximum temperature of the working fluid in the ORC-process should be 100 °C. It can be expected that substances with low critical

Table 1
Equation of state parameters for potential ORC working fluids

| Substance | | α | T_0 (K) | ρ_0 (mol/l) | Q^{*2} | μ^{*2} | BI Ref. | c_p^0 Ref. |
|--|--|----------|-----------|------------------|----------|------------|---------|--------------|
| R32 | CH ₂ F ₂ | 1.2829 | 264.52 | 8.5305 | 1.2150 | 10.568 | [13] | [19] |
| R41 | CH ₃ F | 1.0695 | 238.92 | 9.7506 | 0. | 10.899 | [9] | [24] |
| R125 | CF ₃ -CHF ₂ | 1.4155 | 312.75 | 4.5933 | 3.1327 | 1.0179 | [8] | [19] |
| R134a | CF ₃ -CH ₂ F | 1.4287 | 332.07 | 4.9570 | 2.5882 | 4.6339 | [8] | [19] |
| R143a | CF ₃ -CH ₃ | 1.4128 | 324.54 | 5.2162 | 1.2843 | 4.0775 | [9] | [19] |
| R152a | CHF ₂ -CH ₃ | 1.4137 | 344.88 | 5.7340 | 1.0370 | 5.9951 | [8] | [19] |
| R218 | C ₃ F ₈ | 1.4310 | 309.45 | 3.1611 | 3.7140 | 0.0 | [8] | [18] |
| R227ea | CF ₃ -CHF-CF ₃ | 1.4312 | 334.38 | 3.3083 | 3.9037 | 0.8604 | [12] | [20] |
| R236ea | CF ₃ -CHF-CHF ₂ | 1.1123 | 292.12 | 3.2881 | 6.3908 | 3.7008 | [8] | [21] |
| R236fa | CF ₃ -CH ₂ -CF ₃ | 1.4484 | 350.08 | 3.4559 | 3.9232 | 2.4942 | [12] | [22] |
| R245ca | CF ₃ -CHF-CH ₂ F | 1.4425 | 406.09 | 3.7342 | 3.6130 | 1.3673 | [12] | [22] |
| R245fa | CF ₃ -CH ₂ -CHF ₂ | 1.4395 | 372.51 | 3.6416 | 4.0950 | 2.0612 | [12] | [17] |
| RC270 | Cyclo-propane | 1.2919 | 394.37 | 6.0620 | 0.6844 | 0.0 | [12] | [23] |
| R290 | Propane | 1.3271 | 361.06 | 4.9169 | 1.1230 | 0.0 | [13] | [24] |
| RC318 | Cyclo-C ₄ F ₈ | 1.4497 | 345.63 | 2.9814 | 4.1053 | 0.0 | [12] | [25] |
| R338mccq | CF ₃ -CF ₂ -CF ₂ -CH ₂ F | 1.4553 | 376.42 | 2.6734 | 4.5654 | 0.8479 | [12] | [26] |
| R600 | <i>n</i> -butane | 1.3693 | 411.13 | 3.8553 | 1.7878 | 0.0 | [13] | [24] |
| R600a | Iso-butane | 1.3656 | 392.85 | 3.8145 | 1.7715 | 0.0 | [13] | [24] |
| R1270 | CH ₃ -CH=CH ₂ | 1.3173 | 356.04 | 5.3747 | 1.1502 | 0.0 | [10] | [24] |
| CF ₃ I | CF ₃ I | 1.3629 | 387.51 | 4.3271 | 1.4014 | 0.0 | [12] | [27] |
| C ₅ F ₁₂ | <i>n</i> -perfluoropentane | 2.0011 | 346.50 | 1.4501 | 5.4492 | 0.0 | [14] | [18] |
| R601 | <i>n</i> -pentane | 1.4011 | 448.96 | 3.1407 | 2.3962 | 0.0 | [13] | [18] |
| R601a | Iso-pentane | 1.3851 | 441.29 | 3.1599 | 2.1445 | 0.0 | [13] | [18] |
| neo-C ₅ H ₁₂ | Neo-pentane | 1.3686 | 416.12 | 3.1328 | 1.9078 | 0.0 | [13] | [18] |
| <i>n</i> -C ₆ H ₁₄ | <i>n</i> -hexane | 1.4230 | 480.88 | 2.6919 | 2.9200 | 0.0 | [13] | [18] |
| RE125 | CF ₃ -O-CHF ₂ | 1.4205 | 318.67 | 4.0563 | 3.6631 | 0.8907 | [12] | [28] |
| RE134 | CHF ₂ -O-CHF ₂ | 1.4456 | 379.90 | 4.3682 | 3.9061 | 0.7764 | [12] | [29] |
| RE170 | CH ₃ -O-CH ₃ | 1.3653 | 389.65 | 5.8665 | 1.2569 | 1.5292 | [12] | [24] |
| RE245 | CHF ₂ -O-CH ₂ -CF ₃ | 1.1922 | 337.12 | 3.0966 | 5.9738 | 1.5818 | [12] | [29] |
| RE245mc | CF ₃ -CF ₂ -O-CH ₃ | 1.4361 | 364.38 | 3.1970 | 3.6403 | 2.2965 | [12] | [17] |
| RE347mcc | CF ₃ -CF ₂ -CF ₂ -O-CH ₃ | 1.4161 | 378.16 | 2.4557 | 4.1354 | 1.9019 | [12] | [17] |

Columns 3–7 show the BACKONE parameters, column 8 the references for the BACKONE parameters, and column 9 the references for c_p^0 .

Table 2
Comparison of ORC cycles with pressures up to 20 bar without (–IHE) and with internal heat exchanger (+IHE)

| Substance | Cycle type | T_c (°C) | p_c (bar) | T_3 (°C) | T_4 (°C) | p_{\min} (bar) | p_{\max} (bar) | \dot{m} (kg/s) | \dot{V}_3 (m ³ /s) | \dot{V}_4/\dot{V}_3 | η_{th} , % –IHE | η_{th} , % +IHE | x |
|------------------------------------|------------|------------|-------------|------------|------------|------------------|------------------|------------------|---------------------------------|-----------------------|--------------------------------|--------------------------------|------|
| R125 | b1 | 66.18 | 36.30 | 40.06 | 30.0 | 15.64 | 20.0 | 400.37 | 2.878 | 1.27 | 2.32 | — | 0.99 |
| R125 | b3 | 66.18 | 36.30 | 100.0 | 91.92 | 15.64 | 20.0 | 246.30 | 2.729 | 1.29 | 2.36 | 3.36 | — |
| R218 | o2 | 71.89 | 26.80 | 58.99 | 33.68 | 10.04 | 20.0 | 238.23 | 0.935 | 2.62 | 5.22 | — | — |
| R218 | o3 | 71.89 | 26.80 | 100.0 | 82.86 | 10.04 | 20.0 | 151.55 | 0.968 | 2.15 | 5.15 | 7.50 | — |
| R143a | b1 | 72.73 | 37.64 | 43.59 | 30.0 | 14.40 | 20.0 | 197.92 | 2.084 | 1.18 | 3.14 | — | 0.98 |
| R143a | b3 | 72.73 | 37.64 | 100.0 | 87.37 | 14.40 | 20.0 | 127.89 | 2.013 | 1.39 | 3.31 | 4.36 | — |
| R32 | b1 | 78.11 | 57.83 | 31.36 | 30.0 | 19.31 | 20.0 | 1062.6 | 18.683 | 0.961 | 0.36 | — | 0.99 |
| R32 | b3 | 78.11 | 57.83 | 100.0 | 97.75 | 19.31 | 20.0 | 682.78 | 18.003 | 1.03 | 0.42 | 0.53 | — |
| RE125 | b2 | 81.34 | 33.51 | 57.67 | 31.50 | 10.11 | 20.0 | 145.17 | 0.946 | 2.249 | 5.67 | — | — |
| RE125 | b3 | 81.34 | 33.51 | 100.0 | 79.04 | 10.11 | 20.0 | 103.11 | 0.955 | 2.046 | 5.77 | 7.34 | — |
| R1270 | b1 | 92.42 | 46.65 | 48.54 | 30.0 | 13.09 | 20.0 | 69.334 | 1.580 | 1.173 | 4.28 | — | 0.98 |
| R1270 | b3 | 92.42 | 46.65 | 100.0 | 81.28 | 13.09 | 20.0 | 49.109 | 1.547 | 1.511 | 4.53 | 5.51 | — |
| R290 | b1 | 96.65 | 42.50 | 57.14 | 30.0 | 10.79 | 20.0 | 48.776 | 1.063 | 1.667 | 5.91 | — | 0.99 |
| R290 | b3 | 96.65 | 42.50 | 100.0 | 76.02 | 10.79 | 20.0 | 36.100 | 1.056 | 1.860 | 6.11 | 7.32 | — |
| R134a | b1 | 101.03 | 40.56 | 67.75 | 30.0 | 7.722 | 20.0 | 68.55 | 0.656 | 2.357 | 7.74 | — | 0.99 |
| R227ea | o2 | 101.74 | 29.29 | 83.88 | 44.19 | 5.331 | 20.0 | 81.523 | 0.423 | 4.93 | 9.20 | — | — |
| R152a | b1 | 113.5 | 44.95 | 72.59 | 30.0 | 6.888 | 20.0 | 38.503 | 0.588 | 3.01 | 8.82 | — | 0.96 |
| R152a | b3 | 113.5 | 44.95 | 100.0 | 53.84 | 6.888 | 20.0 | 31.987 | 0.599 | 2.86 | 9.22 | 9.71 | — |
| RC318 | o2 | 115.23 | 27.78 | 98.93 | 54.72 | 3.68 | 20.0 | 66.828 | 0.290 | 7.79 | 10.97 | 12.09 | — |
| RC318 | o3 | 115.23 | 27.78 | 100.0 | 56.38 | 3.68 | 20.0 | 68.694 | 0.305 | 7.67 | 10.55 | 11.75 | — |
| CF ₃ I | b1 | 123.29 | 39.53 | 85.24 | 30.0 | 5.652 | 20.0 | 97.043 | 0.501 | 1.577 | 10.63 | — | 0.96 |
| CF ₃ I | b3 | 123.29 | 39.53 | 100.0 | 39.60 | 5.652 | 20.0 | 86.917 | 0.512 | 3.537 | 10.93 | — | — |
| RC270 | b3 | 124.65 | 54.90 | 100.0 | 41.63 | 8.227 | 20.0 | 24.713 | 0.761 | 2.18 | 8.86 | — | — |
| R236fa | o2 | 125.55 | 32.00 | 100.0 | 48.61 | 3.240 | 19.35 | 47.313 | 0.315 | 7.54 | 11.63 | 12.14 | — |
| RE170 | b1 | 126.85 | 52.40 | 75.10 | 30.00 | 6.733 | 20.0 | 63.068 | 0.580 | 1.578 | 9.38 | — | 0.98 |
| RE170 | b3 | 126.85 | 52.40 | 100.0 | 53.03 | 6.733 | 20.0 | 54.488 | 0.587 | 2.896 | 9.68 | 10.13 | — |
| RE245mc | o2 | 133.68 | 28.87 | 100.0 | 54.50 | 2.416 | 14.88 | 42.549 | 0.411 | 7.314 | 11.84 | 12.72 | — |
| R600a | o2 | 135.05 | 36.50 | 100.0 | 45.33 | 4.038 | 19.98 | 20.423 | 0.359 | 5.854 | 12.12 | 12.43 | — |
| R236ea | o2 | 139.22 | 34.12 | 100.0 | 53.92 | 2.438 | 15.74 | 41.361 | 0.384 | 7.47 | 12.02 | 12.83 | — |
| RE134 | o2 | 147.1 | 42.28 | 100.0 | 41.04 | 2.501 | 16.66 | 32.149 | 0.374 | 7.173 | 12.56 | — | — |
| C ₅ F ₁₂ | o2 | 148.85 | 20.40 | 100.0 | 72.76 | 1.037 | 7.66 | 67.15 | 0.701 | 8.89 | 10.49 | 13.10 | — |
| R600 | o2 | 152.05 | 38.00 | 100.0 | 48.43 | 2.850 | 15.29 | 17.746 | 0.454 | 5.899 | 12.58 | 13.04 | — |
| R245fa | o2 | 154.05 | 36.40 | 100.0 | 50.70 | 1.801 | 12.67 | 33.424 | 0.468 | 7.61 | 12.52 | 13.07 | — |
| R338mccq | o2 | 158.8 | 27.26 | 100.0 | 63.08 | 1.117 | 8.428 | 46.486 | 0.659 | 8.436 | 11.84 | 13.30 | — |
| neo-C ₅ H ₁₂ | o2 | 160.65 | 32.00 | 100.0 | 58.92 | 2.001 | 11.16 | 20.426 | 0.598 | 6.204 | 12.20 | 13.37 | — |
| RE347mcc | o2 | 164.55 | 24.76 | 100.0 | 66.98 | 0.959 | 7.103 | 45.263 | 0.799 | 8.104 | 11.72 | 13.49 | — |
| RE245 | o2 | 170.88 | 30.48 | 100.0 | 58.47 | 1.040 | 8.198 | 42.549 | 0.411 | 8.208 | 12.59 | 13.59 | — |
| R245ca | o2 | 174.42 | 39.25 | 100.0 | 53.75 | 1.230 | 9.343 | 30.548 | 0.619 | 7.88 | 12.79 | 13.47 | — |
| R601a | o2 | 187.75 | 33.86 | 100.0 | 58.47 | 1.098 | 7.223 | 17.439 | 0.865 | 6.793 | 12.75 | 13.76 | — |
| R601 | o2 | 196.5 | 33.70 | 100.0 | 57.74 | 0.828 | 5.963 | 16.331 | 1.007 | 7.274 | 12.91 | 13.84 | — |
| <i>n</i> -hexane | o2 | 234.67 | 30.10 | 100.0 | 61.89 | 0.250 | 2.481 | 15.853 | 2.113 | 9.605 | 13.00 | 14.14 | — |

The condensation temperature is $T_1 = 30^\circ\text{C}$, the internal heat exchanger temperature at the vapour outlet is $T_{4a} = 40^\circ\text{C}$, the isentropic turbine efficiency is $\eta_{sT} = 0.85$, and the isentropic pump efficiency is $\eta_{sP} = 0.65$. The mass and the volume flow rates refer to a power output $|W| = 1\text{ MW}$.

temperatures like R143a ($T_c = 72.73^\circ\text{C}$) have a low η_{th} if the liquid is evaporated at a subcritical pressure. Now the question is whether η_{th} rises if they are compressed to a supercritical pressure. On the other side, the substance with the highest critical temperature is *n*-hexane ($T_c = 234.67^\circ\text{C}$). Here, the idea is to study the influence of the critical temperature on the performance along the homologous series of the *n*-alkanes propane, butane, pentane and hexane.

4. Cycle thermodynamics and thermal efficiencies

All the cycles considered here have a maximum temperature of 100°C and a condensation temperature of

30°C . First, we note that the maximum thermal efficiency η_{th} of a cycle between 30°C and 100°C amounts to 18.8% for the Carnot cycle. In the following, we will consider subcritical and supercritical cycles separately.

4.1. Subcritical pressure cycles

ORC cycles of types b1, b2, b3, o2 and o3 as described in Section 2 and shown in Figs. 1–3 are considered here. The condenser temperature, which is the minimum temperature in the cycle is $T_1 = 30^\circ\text{C}$ and the corresponding vapour pressure is p_{\min} . The highest temperature is T_3 , which occurs at the inlet of the turbine and is limited to $T_3 \leq 100^\circ\text{C}$. Finally, the highest pressure in the cycle is

Table 3
Comparison of ORC cycles with supercritical pressures without (–IHE) and with internal heat exchanger (+ IHE)

| Substance | Cycle type | T_c (°C) | p_c , (bar) | T_3 (°C) | T_4 (°C) | p_{\min} (bar) | p_{\max} (bar) | \dot{m} (kg/s) | \dot{V}_3 (m ³ /s) | \dot{V}_4/\dot{V}_3 | η_{th} , % –IHE | η_{th} , % + IHE | x |
|-----------|------------|------------|---------------|------------|------------|------------------|------------------|------------------|---------------------------------|-----------------------|--------------------------------|---------------------------------|------|
| R41 | s2 | 44.25 | 58.70 | 100.0 | 70.83 | 44.43 | 65.0 | 89.43 | 0.9057 | 1.38 | 3.45 | 4.52 | — |
| R143a | s2 | 72.73 | 37.64 | 100.0 | 51.72 | 14.40 | 40.0 | 56.86 | 0.345 | 3.01 | 8.64 | 9.29 | — |
| R143a | s2 | 72.73 | 37.64 | 100.0 | 42.70 | 14.40 | 45.0 | 57.44 | 0.281 | 3.52 | 9.05 | 9.21 | — |
| R143a | s2 | 72.73 | 37.64 | 100.0 | 33.02 | 14.40 | 50.0 | 61.58 | 0.239 | 4.11 | 9.07 | — | — |
| R143a | s1 | 72.73 | 37.64 | 100.0 | 30.0 | 14.40 | 55.0 | 70.95 | 0.213 | 4.85 | 8.68 | — | 0.93 |
| R143a | s1 | 72.73 | 37.64 | 100.0 | 30.0 | 14.40 | 60.0 | 87.60 | 0.203 | 5.68 | 7.92 | — | 0.84 |
| R290 | s1 | 96.65 | 42.50 | 100.0 | 30.0 | 10.80 | 50.0 | 60.34 | 0.190 | 8.816 | 7.39 | — | 0.63 |

The condensation temperature is $T_1 = 30^\circ\text{C}$, the heat exchanger temperature at the vapour outlet is $T_{4a} = 40^\circ\text{C}$, the isentropic turbine efficiency is $\eta_{sT} = 0.85$, and the isentropic pump efficiency is $\eta_{sP} = 0.65$. The mass and the volume flow rates refer to a power output $|\dot{W}| = 1\text{ MW}$.

the evaporator pressure p_{\max} which is limited to $p_{\max} \leq 20$ -bar. If an IHE is used, then we assume that the temperature at the outlet of the IHE on the low pressure side is 10°C higher than the condenser temperature, i.e. $T_{4a} = 40^\circ\text{C}$. Finally, the isentropic efficiencies for the pump and the turbine were assumed to be $\eta_{sP} = 0.65$ and $\eta_{sT} = 0.85$, respectively.

Details of the cycles for 30 working fluids are displayed in Table 2. It includes the type of the cycle in the T_s -diagram, the critical temperature T_c and pressure p_c , the state point at the inlet of the turbine (T_3, p_{\max}) and at the outlet of the turbine (T_4, p_{\min}). Moreover, Table 2 contains the mass flow rate \dot{m} and the volume flow rate at the turbine inlet \dot{V}_3 for 1MW output power, the turbine outlet/inlet volume flow ratio \dot{V}_4/\dot{V}_3 , the thermal efficiency η_{th} without and with IHE, and the vapour content x after the expansion in the turbine in case of wet vapour. As a convenient introduction to Table 2 we give explanations for three cycles.

Case 1: b1 cycle without IHE for R152a. Point 1 is on the saturated liquid line at $T_1 = 30^\circ\text{C}$ and the corresponding saturation pressure $p_{\min} = 6.888$ bar. Point 3 is on the saturated vapour line at $p_{\max} = 20$ bar and the corresponding saturation temperature $T_3 = 72.59^\circ\text{C}$. The working fluid is expanded in the evaporator to point 4 where it reaches p_{\min} in the two-phase region at temperature $T_1 = 30^\circ\text{C}$ and vapour content $x = 0.96$. Then it enters directly the condenser.

Case 2: b3 cycle for R152a. Starts as case 1 but point 3 is vapour superheated to $T_3 = 100^\circ\text{C}$.

Case 3: o2 cycle with IHE for R236ea. Point 3 is on the saturated vapour line at $T_3 = 100^\circ\text{C}$ and the corresponding saturation pressure $p_{\max} = 15.74$ bar. Point 4 is superheated vapour at temperature $T_4 = 53.92^\circ\text{C}$ which is cooled down in an IHE to $T_{4a} = 40^\circ\text{C}$ before it enters the condenser.

We first observe, that the fluids consisting of simpler molecules are mostly of type b whilst those consisting of more complicated molecules are mostly of type o. Moreover, as in general, the molecularly simpler fluids have lower critical temperatures T_c , we find for lower T_c mostly b-fluids and for higher T_c mostly o-fluids.

As a consequence, the b-fluids considered evaporate at 20 bar at temperatures lower than 100°C . Then one can decide whether the saturated vapour shall enter the turbine directly or whether it should be superheated to 100°C . In the first case we have cycles of type b1 or b2—which only occurs for RE125—, in the second case we have cycles of type b3. We learn from Table 2 that the thermal efficiency η_{th} is always higher with superheating than without. Whilst this increase of η_{th} by superheating without using an IHE is in general small, a more significant increase can be achieved if superheating is combined with an IHE. The general trend is that with increasing critical temperature, the thermal efficiency η_{th} increases. The largest η_{th} values are achieved for R152a, RE170, and CF3I and range from 9% to 11%.

Regarding the o-fluids in Table 2, most of them have comparatively high critical temperatures. As a consequence the vapour pressures at 100°C are lower than 20 bar. In these cases, the vapour pressures at 100°C are the maximum pressures in the cycle, and the cycles are all of o2-type. Superheating and hence o3 cycles are possible only in case that the saturation temperature at 20 bar is lower than 100°C which occurs for R218, R227ea, and RC318. For R227ea we did not consider superheating to 100°C because that state point is in the critical region. For the other two substances, R218 and RC318, we make the interesting observation that the o3-cycles with superheating yield lower η_{th} values than the o2-cycles without superheating. For all o-fluids with critical temperatures above 100°C we get η_{th} values from 9.2% (R227ea) up to 14.1% (*n*-hexane), which has to be compared with the Carnot value of 18.8% mentioned already above.

So far, we have concentrated only on the thermal efficiencies. For the design of the turbine, however, also the volume flow rate \dot{V}_3 at the inlet of the turbine and the outlet/inlet volume flow ratio \dot{V}_4/\dot{V}_3 are important which are also given in Table 2. For convenience of the reader, some of the results contained in Table 2 are also presented graphically in Figs. 6 and 7. Fig. 6 shows the thermal efficiency η_{th} via the volume flow rate \dot{V}_3 at the inlet of the turbine for a power output $|\dot{W}| = 1\text{ MW}$ and Fig. 7 shows the thermal efficiency η_{th} via the turbine outlet/inlet volume

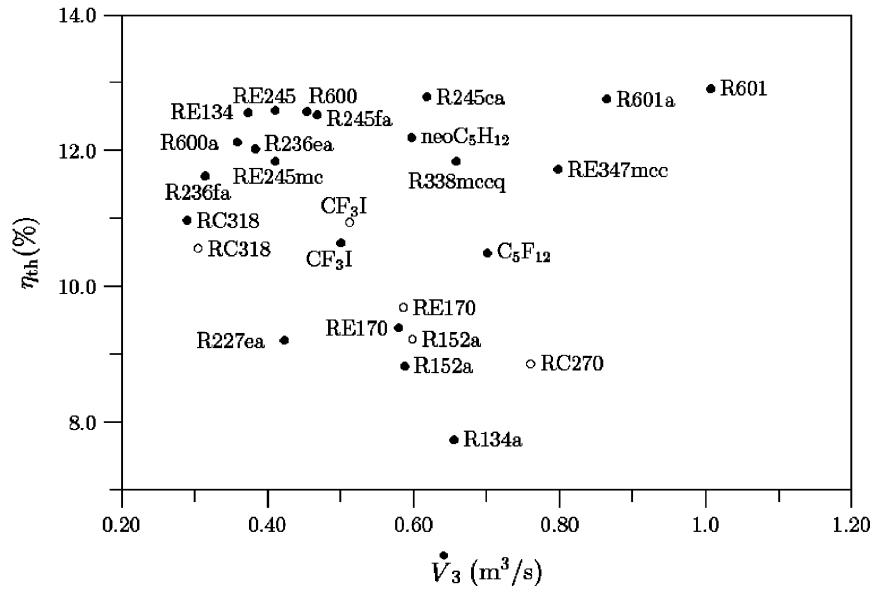


Fig. 6. Thermal efficiency η_{th} vs. volume flow rate \dot{V}_3 at the inlet of the turbine for ORC cycles without internal heat exchanger for selected working fluids. ● without, ○ with superheating.

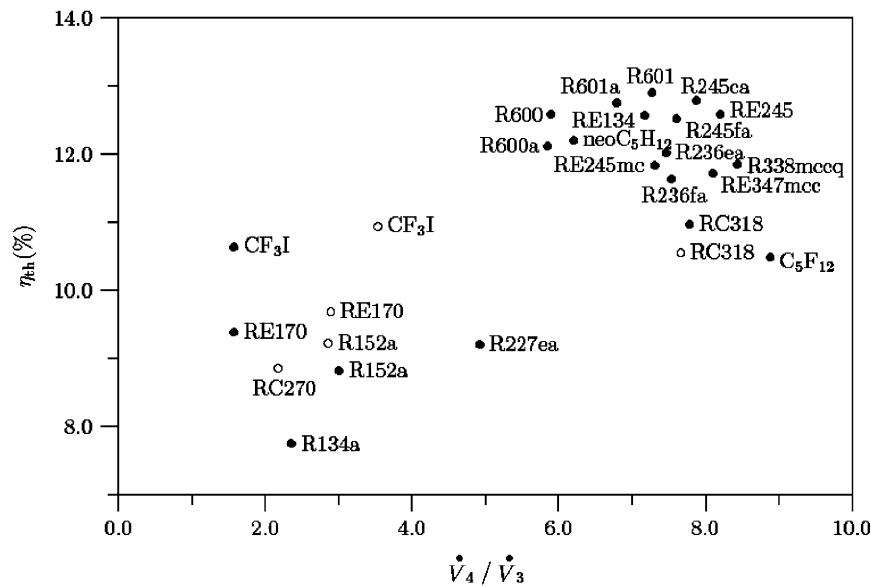


Fig. 7. Thermal efficiency η_{th} vs. turbine outlet/inlet flow ratio \dot{V}_4 / \dot{V}_3 for ORC cycles without internal heat exchanger for selected working fluids. ● without, ○ with superheating.

flow ratio \dot{V}_4 / \dot{V}_3 , both for selected working fluids and cycles without IHE. The corresponding results for the cycles with IHE would occur at the same abscissa values for \dot{V}_3 and \dot{V}_4 / \dot{V}_3 but have somewhat higher η_{th} values which, however, can be found in Table 2. Substances with a high thermal efficiency η_{th} , a low value of \dot{V}_3 and a low value of \dot{V}_4 / \dot{V}_3 are R236ea, R245ca, R245fa, R600, R600a, R601a, RE134, and RE245.

It still might be interesting to consider η_{th} , \dot{V}_3 , and \dot{V}_4 / \dot{V}_3 for the homologous series of *n*-alkanes, i.e. for propane (R290), *n*-butane (R600), *n*-pentane (R601), and *n*-hexane. We observe a dramatic jump in η_{th} (without IHE) from 6.11 for propane to 12.58 for *n*-butane with

subsequent slow increase for the higher alkanes *n*-pentane and *n*-hexane. On the other hand, *n*-pentane has already high values for \dot{V}_3 and for \dot{V}_4 / \dot{V}_3 which are still higher for *n*-hexane. Hence, *n*-butane is considered to be among the *n*-alkanes the most suitable working fluid for the ORC cycle under the prescribed conditions. Supplementary calculations show that increasing the temperature T_3 at the turbine inlet from 100 °C to higher temperatures, the higher alkanes *n*-pentane and subsequently *n*-hexane become better suitable as working fluids from a thermodynamic point of view (a certain problem at too high temperatures, however, lies in their auto ignition as will be discussed below).

4.2. Supercritical pressure cycles

Here we consider ORC-cycles of type s1 and s2 as described in Section 2 and shown for s1 in Fig. 4. Substances with low critical temperatures like R143a ($T_c = 72.73^\circ\text{C}$) yield in b1 and b3 cycles with $p_{\max} = 20$ bar low thermal efficiencies and it is interesting to study their behaviour again in the temperature range between 100 and 30°C if they are compressed to a supercritical pressure. In addition to R143a we studied also R41 with a lower critical temperature ($T_c = 44.25^\circ\text{C}$) and R290 with a higher critical temperature ($T_c = 96.65^\circ\text{C}$). The critical quantities of these fluids (T_c, p_c), the state points of the cycles ($T_3, T_4, p_{\min}, p_{\max}$), the mass and volume flow rates (\dot{m}, \dot{V}_3 and \dot{V}_4/\dot{V}_3) referring to 1 MW output power, the thermal efficiency (η_{th}) and the vapour content in case of s1 are given in Table 3.

For a detailed understanding let us first consider the s2-cycle of R143a at 40 bar which is slightly above the critical pressure ($p_c = 37.64$ bar). Table 3 shows that point 1 is on the saturated liquid line at $T_0 = 30^\circ\text{C}$ with the corresponding saturation pressure $p_{\min} = 14.40$ bar. Point 3 is in the superheated region at $T_3 = 100^\circ\text{C}$ and the supercritical isobar $p_{\max} = 40$ bar. The working fluid enters the turbine at point 3 and is expanded to point 4 where it reaches p_{\min} as superheated vapour at temperature $T_4 = 51.72^\circ\text{C}$. Then it either enters directly the condenser yielding $\eta_{\text{th}} = 8.64\%$ or it is cooled to $T_{4a} = 40^\circ\text{C}$ by an IHE before it enters the condenser yielding $\eta_{\text{th}} = 9.29\%$. With this supercritical pressure the thermal efficiency increases by more than a factor 2 compared with the subcritical cycle with $p_{\max} = 20$ bar. Increasing the supercritical pressure to 50.0 bar shifts the state points 3 and 4 in the T, s -diagram to the left and the working fluid leaves the turbine still as superheated vapour at temperature $T_4 = 33.02^\circ\text{C}$ yielding $\eta_{\text{th}} = 9.07\%$ without IHE. Further increase of the pressure to 60 bar shifts points 3 and 4 further to the left in the T, s -diagram with the results that point 4 ($p_{\min} = 14.40$ bar, $T_4 = 30.0^\circ\text{C}$) lies in the two-phase region with the low vapour content $x = 0.84$; this corresponds to a s1-cycle as shown in Fig. 4. The thermal efficiency η_{th} decreases to 7.92% mainly because the enthalpy of point 3 decreases significantly with this increase of the pressure. We conclude that the best thermal efficiencies for R143a are found at slightly supercritical pressures (p_{\max} between 40 and 50 bar) and have values of about 9%. Lower pressures ($p_{\max} = 20$ bar) or higher pressures (60 bar or higher) yield smaller thermal efficiencies.

Regarding R143a we see that its critical temperature is close to the average temperature of the considered ORC cycles with temperatures ranging from 100 to 30°C . The question arises then about thermal efficiencies of supercritical cycles with working fluids having lower or higher critical temperatures. Results for calculations with R41 ($T_c = 44.25^\circ\text{C}$) and R290 ($T_c = 96.65^\circ\text{C}$) are also presented in Table 3. We learn that R41 has at slightly supercritical pressure a rather low thermal efficiency. On

the other hand, a cycle with R290 yields a state point 4, which is rather wet ($x = 0.63$).

Summarizing we can say that supercritical cycles of type s2 of appropriately chosen substances as R143a show similar thermal efficiencies (about 9%) and similar low volume ratios \dot{V}_4/\dot{V}_3 as the subcritical b1 and b3 cycles of substances as R152a. The advantage of supercritical R143a over subcritical R152a is the small volume flow rate \dot{V}_3 at the entrance of the turbine (0.3 vs. $0.6\text{ m}^3/\text{s}$).

5. Heat transfer from the heat carrier to the working fluid

It has already been mentioned in Section 2 that the heat transfer from the heat carrier to the working fluid has also to be considered to get a maximum power output in an ORC cycle from a given heat source. The EHE is shown schematically in Fig. 5. Let us assume that the mass flow rate of the heat carrier is \dot{m}_c and that it enters the EHE at state point 5 with temperature $T_5 > T_3$ and leaves it at state point 6 with temperature T_6 . Then the heat flow rate transferred without loss to the working fluid is $\dot{Q}_{\text{in}} = \dot{m}_c q_{56}$. The decisive item is now that the minimum temperature T_6 to which the heat carrier is cooled down in the EHE is determined by the temperature vs. enthalpy flow $T, \Delta\dot{H}$ -diagram of the working fluid in the evaporator or, with other words, by a pinch point analysis.

Here, we show $T, \Delta\dot{H}$ -diagrams in the evaporator for three representative ORC cycles of Tables 2 and 3 with power output $|\dot{W}|$ of 1 MW. The diagrams are given in Fig. 8 for R601 in the o2-cycle, in Fig. 9 for R152a in the b3-cycle and in Fig. 10 for R143a in a s2-cycle at 45 bar.

For the further discussion let us assume that the heat carrier enters the EHE with $T_5 = 120^\circ\text{C}$, that the pinch

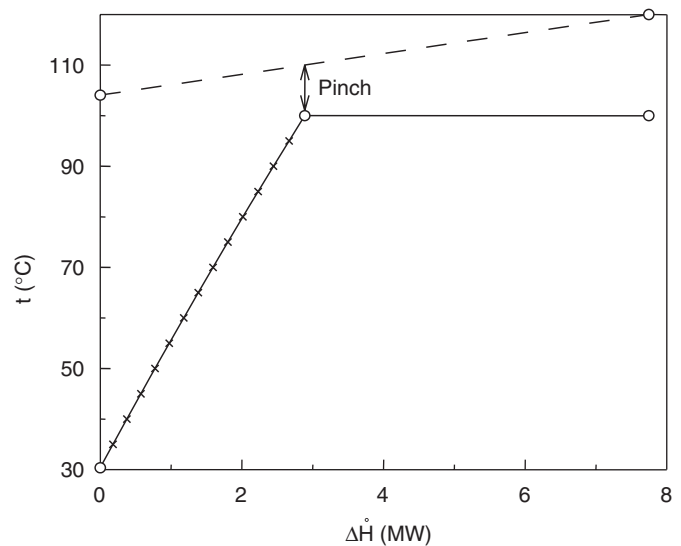


Fig. 8. $T, \Delta\dot{H}$ -diagram for heating R601 in a b1-cycle at 5.963 bar from state point 2 ($T = 30.37^\circ\text{C}$) to state point 3 (100°C).

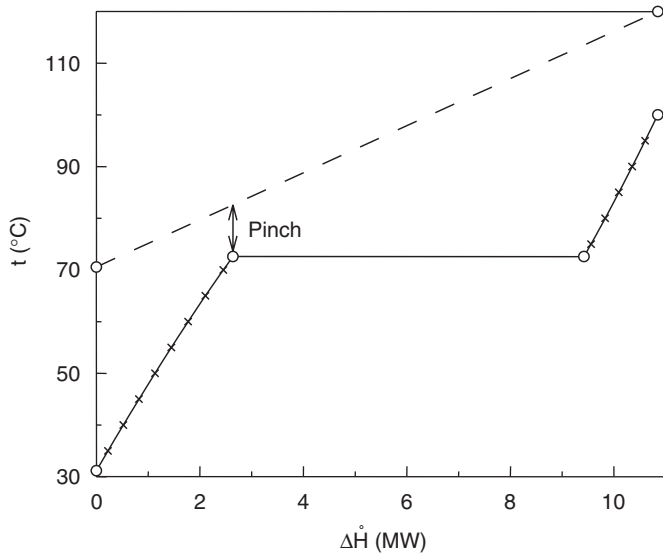


Fig. 9. $T, \Delta \dot{H}$ –diagram for heating R152a in a b3-cycle at 20 bar from state point 2 ($T = 31.16^\circ\text{C}$) to state point 3 (100°C).

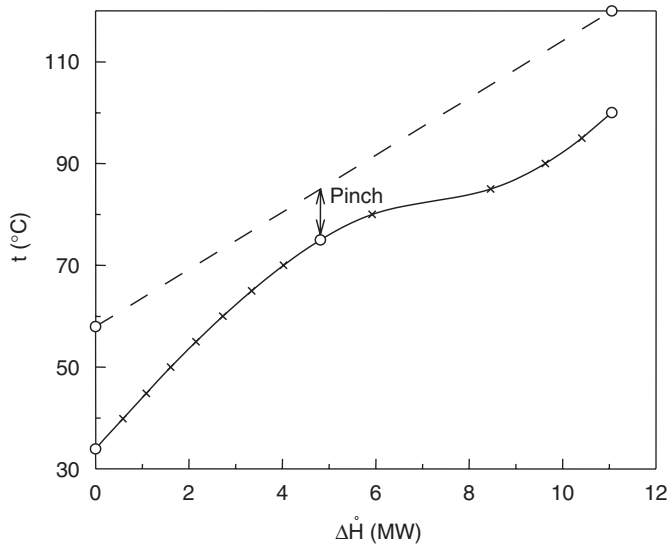


Fig. 10. $T, \Delta \dot{H}$ –diagram for heating R143a in a s2-cycle at 45 bar from state point 2 ($T = 33.93^\circ\text{C}$) to state point 3 (100°C).

point temperature difference $\Delta T_p = 10^\circ\text{C}$ and that the heat capacity of the heat carrier $c_{p,c} = 4.2 \text{ kJ/kg K}$ and constant. For R601, e.g., it is evident from Fig. 8 that the pinch point temperature of the cold fluid is $T_{p,c} = 100^\circ\text{C}$ and that of the hot fluid is $T_{p,h} = 110^\circ\text{C}$. Consequently, the heat carrier fluid is cooled down at the outlet of the EHE to only $T_6 = 104.05^\circ\text{C}$, the transferred heat per mass unit of the heat carrier is $q_{56} = 66.99 \text{ kJ/kg}$, and in order to produce a power output $|\dot{W}|$ of 1 MW without IHE ($\eta_{th} = 0.1291$) a heat carrier mass flow rate $\dot{m}_c = |\dot{W}|/(q_{56}\eta_{th}) = 115.6 \text{ kg/s}$ is required. The same analysis was also made for C₅F₁₂, for R152a with overheating as well as for R143a compressed to 45 bar, all without IHE. The results are compiled in Table 4.

We see immediately from Table 4 that the required heat carrier mass flow rate is the smallest for the s2-cycle of R143a with the thermal efficiency $\eta_{th} = 0.0905$ and is much larger for the o2-cycle of C₅F₁₂ and even larger for the o2-cycle of R601 with the highest thermal efficiency $\eta_{th} = 0.1291$. Hence, the crucial question, which working fluid should be used in an ORC cycle, does not only depend on its thermal efficiency but also on the supply and the further processing of the heat carrier fluid. Without being complete, we mention three different possibilities for this supply and processing.

- (a) The heat carrier is water, which is heated up in a solar collector and circulates in a loop. After it has gone through the EHE it is reheated in the solar collector from T_6 to T_5 by just adding the heat flow $\dot{Q}_{in} = |\dot{W}|/\eta_{th}$. In this case, working fluids with high thermal efficiencies like R601 are favourable.
- (b) The heat carrier is water from a geothermal source and after it has gone through the EHE it is discharged into the environment or fed back into the underground. In this case one is interested to have a maximum power output $|\dot{W}|$ from a minimum mass flow rate of the heat carrier fluid. From $|\dot{W}| = \dot{m}_c q_{56} \eta_{th}$ it follows that a combination of a high thermal efficiency η_{th} and a low outlet temperature T_6 of the heat carrier is favourable.

Table 4

Pinch analysis of the external heat exchanger (EHE) for three representative ORC cycles corresponding to Figs. 11–13 and for the o2-cycle of C₅F₁₂. All cycles are for a power output $|\dot{W}| = 1 \text{ MW}$ and without IHE

| Substance | Cycle type | $T_{p,c}$ ($^\circ\text{C}$) | $T_{p,h}$ ($^\circ\text{C}$) | T_6 ($^\circ\text{C}$) | q_{56} (kJ/kg) | η_{th} (%) | \dot{m}_c (kg/s) |
|--------------------------------|-----------------|--------------------------------|--------------------------------|----------------------------|------------------|-----------------|--------------------|
| R601 | o2 | 100.0 | 110.0 | 104.05 | 67.0 | 12.91 | 115.6 |
| C ₅ F ₁₂ | o2 | 100.0 | 110.0 | 97.24 | 95.59 | 10.49 | 99.7 |
| R152a | b3 | 72.59 | 82.59 | 70.57 | 207.6 | 9.22 | 52.2 |
| R143a | s2 ^a | 75.00 | 85.00 | 57.97 | 260.5 | 9.05 | 42.4 |

The heat carrier fluid enters the EHE with $T_5 = 120^\circ\text{C}$.

^a45 bar.

It is interesting to note that among the cycles considered in Table 4, the supercritical cycle with R143a requires the smallest heat carrier mass flow rate \dot{m}_c .

- (c) In case of a high heat carrier outlet temperature T_c as for R601 one might also think about a second stage ORC cycle. This might e.g. be the considered b3-cycle for R152a or the s2-cycle for R143a.

6. Additional aspects

So far, we have considered the thermodynamic aspects of potential working fluids for ORC processes. Other points of interest for ORC cycles are environmental and safety aspects of the working fluids as well as their chemical stability, which shall be discussed here only briefly.

Environmental aspects are the ozone depletion potential (ODP), the global warming potential (GWP) and the atmospheric lifetime (ALT). These properties are given for many of the working fluids considered here in Ref. [5]. Perfluoropentane used in existing geothermal plants [3,4] has a very high GWP of 9010 with respect to carbon dioxide and an ALT of 4100 years [5]. Thus, many other working fluids are thought to be a better choice since perfluoropentane has only a medium thermal efficiency $\eta_{th} = 10.49$ (without IHE) combined with a high pinch point temperature $T_{p,c} = 100.0$ °C in the present case study.

Regarding the safety aspects, the flammability and the auto ignition have to be mentioned. For sure, many of the substances considered are flammable but this does not seem to be a serious problem because in existing ORC processes at even higher temperatures R601 is used as working fluid [30]. Auto ignition seems to be a problem, in particular, for longer alkanes at temperatures above 200 °C. For many substances the degree of flammability and the auto ignition temperature can be found on safety data sheets, as e.g. for *n*-pentane (R601) in Ref. [31].

A frequently questioned point is that of the chemical stability of the considered working fluids. Whilst we do not yet know a comprehensive investigation of that topic, it seems that for alkanes this is not a serious problem again because e.g. *n*-pentane is used in ORC processes already for long time at even higher temperatures [30].

7. Summary and conclusions

In the present paper, mostly thermodynamic aspects of potential working fluids for ORC processes calculated on the basis of the BACKONE equation of state have been considered. In Section 4, Tables 2 and 3 and Figs. 6 and 7, we have shown thermal efficiencies and other important properties as volume flow rates. Moreover, in Section 5, Table 4 and Figs. 8–10, we have performed a pinch point analysis for the external heat exchanger and discussed the consequences for an optimized use of the heat source.

Interesting findings concern the superheating of the vapour. For the b-cycles it was found that the increase of the thermal efficiency η_{th} by superheating is only small in the case without IHE and hence not really rewarding. A more significant increase can be achieved if superheating is combined with an IHE. At the contrary, for the o-cycles we found a decrease of the thermal efficiency by superheating.

Another interesting observation is that fluids with low T_c are mostly b-fluids whilst those with higher for higher T_c are mostly o-fluids. This means that for ORC-processes at higher temperatures than considered here mainly o-processes have to be expected.

A general recommendation for an optimal ORC working fluid requires consideration of the maximum temperature of the working fluid as was discussed in Section 4 for the example of the homologous series of the *n*-alkanes. Moreover, the processing of the heat carrier fluid has also to be taken into account as was pointed out in Section 5. The following recommendations are for the maximum temperature of 100 °C for the working fluid as was assumed throughout this study.

In case the working fluid is reheated in a closed cycle, as e.g. with solar collectors, one might require a high thermal efficiency η_{th} , a low value of \dot{V}_3 and a low value of \dot{V}_4/\dot{V}_3 . In this case one should consider R236ea, R245ca, R245fa, R600, R600a, R601a, RE134, and RE245.

In geothermal use the heat carrier water is discharged into the environment or fed back into the underground after having gone through the external heat exchanger. Hence, one might require for a given heat carrier flow rate \dot{m}_c a maximum output $|\dot{W}|$. The present study for pure working fluids has shown that fluids with lower critical temperatures as R143a in a s2 or R152a in a b3 process are favourable because they yield a more uniform increase of the $T, \Delta\dot{H}$ -curve during heating. Whilst we have investigated only pure fluids here, we believe that mixtures could be an interesting alternative in this case. We want to mention that BACKONE describes also mixtures with high accuracy [7,11].

Finally, we want to mention that for further calculations of thermodynamic properties of pure working fluids EXE-files of BACKONE are available from the corresponding author.

Acknowledgements

The authors thank S. Köhler, Geoforschungszentrum Potsdam, T. Schrag, dezentral energietechnik Berlin, E. Broßmann, Bewag-Vattenfall Berlin, and F. Kabus, Geothermie Neubrandenburg, for fruitful discussions.

References

- [1] Rogers G, Mayhew Y. Engineering thermodynamics, work and heat transfer, 4th ed. Harlow: Longman Scientific & Technical; 1992 (p. 239–243).

- [2] Gaia M. The Altheim Rankine cycle TURBOGENERATOR, 1MW_{el} organic Rankine cycle power plant powered by low temperature geothermal water. In: Geothermische Vereinigung, Geeste, editor. *Geothermische Energie*, vol. 36/37(3/4); 2002. See also: http://www.geothermie.de/gte/gte36-37/altheim_gaia.htm
- [3] Köhler S, Saadat A. Möglichkeiten und Perspektiven der geothermischen Stromerzeugung. In: Huenges E, Saadat A, Köhler S, Rockel W, Hurter S, Seibt A, Naumann D, Zimmer M, Erzinger J, Wiersberg Th, Legarth B, Wolff H, editors. *Geothermische Technologieentwicklung: geologische und energietechnische Ansatzpunkte*, GeoForschungs-Zentrum Potsdam, Scientific Technical Report STR00/23, 2000, p. 7–28 (in German). See also: <http://www.gfz-potsdam.de/pb5/pb52/publicat/reports/report6/gtr0601.pdf>
- [4] Broßmann E, Eckert F, Möllmann G. Technisches Konzept des Kraftwerkes Neustadt-Glewe. In: *Geothermische Vereinigung und GeoForschungsZentrum Potsdam, editors. Start in eine neue Energiezukunft. Tagungsband 1. Fachkongress Geothermischer Strom 12–13 November 2003, Neustadt-Glewe, ISBN 3-932570-49-9, Geeste 2003 (in German)*. See also: <http://www.geothermie.de/ng-brossmann.pdf>
- [5] US Environmental Protection Agency. Global warming potentials of ODS substitutes. Washington, DC: US Environmental Protection Agency, 2006. See also <http://www.epa.gov/docs/ozone/geninfo/gwps.html>
- [6] Müller A, Winkelmann J, Fischer J. Backone family of equations of state: 1. Nonpolar and polar pure fluids. *AIChe J* 1996;42:1116–26.
- [7] Weingerl U, Wendland M, Fischer J, Müller A, Winkelmann J. Backone family of equations of state: 2. Nonpolar and polar fluid mixtures. *AIChe J* 2001;47:705–17.
- [8] Calero S, Wendland M, Fischer J. Description of alternative refrigerants with BACKONE equations. *Fluid Phase Equilib* 1998;152:1–22.
- [9] Wendland M, Calero S, Weingerl U, Fischer J. Beschreibung alternativer Kältemittel und ihrer Gemische mit BACKONE-Gleichungen. *Chem-Ing-Tech* 2000;72:738–42 (in German).
- [10] Saleh B, Weingerl U, Wendland M. Description of the thermodynamic properties of natural refrigerants with BACKONE equations. In: *Proceedings of the IIR conference on thermophysical properties and transfer processes of new refrigerants, 2001 October 3–5; Paderborn, Germany, Paris: International Institute of Refrigeration, 2001, p. 31–8*.
- [11] Wendland M, Saleh B, Fischer J. Accurate thermodynamic properties from the BACKONE equation for the processing of natural gas. *Energy Fuels* 2004;18:938–51.
- [12] Saleh B, Wendland M. Screening of pure fluids as alternative refrigerants. *Int J Refrig* 2006;29:260–9.
- [13] Wendland M. Application of the BACKONE equations of state to quadrupolar fluids. *Fluid Phase Equilib* 2005, submitted for publication.
- [14] Saleh B, Fischer J, Wendland M. BACKONE equation for perfluorinated pentane. Report for dezentral München and Geo-forschungszentrum Potsdam, Institut für Verfahrens- und Energietechnik, Universität für Bodenkultur Wien, 2005.
- [15] Hammer H, Röhmfeld M. Abwärmenutzung zur Krafterzeugung mittels neuer Kreislaufmedien. *VDI-Bericht* 415, 81–87, VDI-Verlag Düsseldorf; 1981 (in German).
- [16] Lemmon EW, McLinden MO, Huber ML. NIST reference fluid thermodynamic and transport properties-REFPROP. NIST standard reference database 23—Version 7.0, 2002.
- [17] Reid RC, Prausnitz JM, Poling BE. *The properties of gases and liquids*, 4th ed. New York: McGraw-Hill; 1987 (p. 154–157).
- [18] Prausnitz JM, Poling BE, O’Connell JP. *The properties of gases and liquids*, 5th ed. New York: McGraw-Hill; 2001 (p. A.35–A.46).
- [19] McLinden MO. Thermodynamic properties of CFC alternatives: A survey of the available data. *Int J Refrig* 1990;13:149–62.
- [20] Benedetto G, Gavioso RM, Spagnolo R, Grigiante. Vapor-phase Helmholtz equation for HFC-227ea from speed-of-sound measurements. *Int J Thermophys* 2001;22:1073–88.
- [21] Defibaugh DR, Gillis KA, Moldover MR, Schmidt JW, Weber LA. Thermodynamic properties of CF₃-CHF-CHF₂, 1,1,1,2,3,3-hexafluoropropane. *Fluid Phase Equilib* 1996;122:131–55.
- [22] Gillis KA. Thermodynamic properties of seven gaseous halogenated hydrocarbons from acoustic measurements: CHClFCF₃, CHF₂CF₃, CF₃CH₃, CHF₂CH₃, CF₃CHFCHF₂, CF₃CH₂CF₃, and CHF₂CF₂CH₂F. *Int J Thermophys* 1997;18:73–135.
- [23] Lide DR, editor. *CRC handbook of chemistry and physics*. 75th ed. Baton Raton: CRC Press; 1995. p. 5–53.
- [24] Reid RC, Prausnitz JM, Poling BE. *The properties of gases and liquids*, 4th ed. New York: McGraw-Hill; 1987 (p. 656–732).
- [25] Platzer B, Polt A, Maurer G. *Thermophysical properties of refrigerants*. Berlin: Springer; 1990 (p. 107–136, 383–411).
- [26] Defibaugh DR, Carrillo-Nava E, Hurly JJ, Moldover MR, Schmidt JW, Weber LA. Thermodynamic properties of HFC-338mccq, CF₃CF₂CF₂CH₂F, 1,1,1,2,2,3,3,4-octafluorobutane. *J Chem Eng Data* 1997;42:488–96.
- [27] Duan YY, Shi L, Sun Q, Zhu MS, Han LZ. Thermodynamic properties of trifluoroiodomethane (CF₃I). *Int J Thermophys* 2000;21:393–404.
- [28] Hurly JJ, Schmidt JW, Gillis KA. Virial equation of state and ideal-gas heat capacities of pentafluoro-dimethylether. *Int J Thermophys* 1997;18:137–59.
- [29] Gillis KA. Thermodynamic properties of two gaseous halogenated ethers from speed-of-sound measurements: Difluoromethoxy-difluoromethane and 2-difluoromethoxy-1,1,1-trifluoroethane. *Int J Thermophys* 1994;15:821–47.
- [30] Bayerisches Landesamt für Umweltschutz. *Niedertemperaturverstromung mittels einer ORC-Anlage im Werk Lengfurt der Heidelberger Zement AG. Endbericht 2001. Order number: lfu_klima_00009. Bayerisches Landesamt für Umwelt, Augsburg. (in German)*. See also: www.bayern.de/lfu/bestell/orc_endbericht.pdf
- [31] Aug. Hedinger GmbH&CoKG. *EG-Sicherheitsdatenblatt: n-Pentan: Stand 24.03.2004. Stuttgart: Aug. Hedinger GmbH&CoKG, 2006 (in German)*. See also: http://hedinger.de/bilder/6/Pentan_n_v003.pdf